Gervas Franceschini
Transmissions, Structures and Drives,
Rolls-Royce plc,
Derby DE24 8BJ, UK
e-mail: gervas.franceschini@rolls-royce.com

Terry V. Jones

David R. H. Gillespie[1]
e-mail: david.gillespie@eng.ox.ac.uk

Department of Engineering Science,
University of Oxford,
Oxford OX1 3PJ, UK

Improved Understanding of Blow-Down in Filament Seals

Brush seals are used to provide flow resistance between rotating and stationary components in gas turbines. Compliant filament seals, such as brush seals, exhibit a phenomenon called blow-down, where the filaments deflect toward the rotor surface when a differential pressure is applied across the seal. This phenomenon is desirable as it enables seal contact to be maintained during rotor contractions and eccentric excursions. This paper describes an aerodynamic mechanism, which can cause the blow-down of bristles. Importantly it shows that distortion of the bristle pack is not necessary to achieve blow-down. Experimental and computational investigations of a large scale model representative of a section of a brush seal are also reported. The measured and predicted detailed pressure distributions thus obtained are used to validate the model of blow-down presented. [DOI: 10.1115/1.3213552]

1 Introduction

A class of adaptable seal comprising angled compliant filaments has been developed for turbine applications over the past 30 years. One of the most well-known of this class is the brush seal. A brush seal is a flexible flow restriction created by the arrangement of numerous fine bristles in close proximity to a rotating shaft [1]. The bristles are usually supported by a backing plate so that the seal operates under elevated differential pressures in a turbine environment. The ability of brush seals to operate effectively at high shaft speeds, temperatures, and with relative radial and axial movements has led to them being employed in many rotating turbomachinery applications where traditional contacting seals do not function [2–4]. The potential advantages of brush seals over the multiple-finned labyrinth seal in terms of thrust or specific fuel consumption are well known [5].

The key feature that makes brush seals adaptable is their blow-down characteristic. The bristles of a brush seal move toward the shaft surface in response to a pressure difference [5]. Blow-down is an aerodynamic phenomenon in which the flow of fluid through the seal generates a force, which causes the compliant elements to move radially inwards. The presence of blow-down can manifest itself as a reduction in leakage or even an increase in seal torque (representing an increase in bristle tip loading). Hence, excessive blow-down can lead to contact wear between the bristles and shaft through elevated bristle-to-rotor loading. The essential mechanisms by which the bristles are blown into contact with the shaft are by no means fully understood. In fact, brush seals are not the only compliant seal, which exhibit the phenomenon of blow-down: the presence of an aerodynamic blow-down force has been noted with leaf seals [6]. This paper identifies an aerodynamic mechanism for generating a blow-down force on angled compliant elements. In the first instance, zero thickness flexible elements are considered. Then the case of finite thickness elements is addressed, specifically with a large scale brush seal bristle pack.

2 Theoretical Justification of Blow-Down

It is the hypothesis of this paper that blow-down is largely an aerodynamic effect experienced by seals whose compliant elements lie primarily in an axial plane and are angled to the radial direction. By considering a simple control volume, it is apparent that both the pressure distribution and flow momentum contribute to blow-down, as described below.

Consider a control volume around a seal made from angled flexible elements, as shown in Fig. 1. The control volume extends sufficiently far upstream for swirl not to be significant (typical of experimental facilities). The control surface is just above the shaft surface and below the casing surface and just ahead of the backing plate, as illustrated. The flexible elements penetrate the control surface. The outlet flow in the gap between the backing plate and the shaft surface contains swirl. The flow through the side surfaces must balance due to periodicity.

The influence of the pressure distribution may be seen by resolving the vertical (or radial) forces in the momentum equation. The pressure acting against the top of the control volume (by the bristle root) is largely the upstream static pressure (p_{up}), while that acting on the lower face (under the bristle tips) is a distribution ranging from the upstream to downstream static pressure. This distribution can be expressed as some fraction of the upstream and downstream pressures $p_{up}-a(p_{up}-p_{down})$ (where $0<a<1$). The driving force per unit area for blow-down then becomes $a(p_{up}-p_{down})$. Essentially this demonstrates that the aerodynamic blow-down effect is driven by differential pressure ΔP rather than pressure ratio. Applying the momentum equation for steady flow conditions suggests that the net momentum flux out of the control volume in the vertical direction should balance this force plus any body forces in the control volume plus the shear force against the backing ring. The presence of a driving radial pressure gradient has been confirmed by experimental and numerical studies [7–11], suggesting near-vertical accelerating flow along the backing ring toward the clearance region.

The influence of flow momentum changes is apparent from the swirl at the exit of the control volume. This indicates that there is angular momentum out but there is no flow angular momentum in. Given that the pressure forces on the side faces of the control volume balance then there is no couple arising from the pressure forces. The only source of a couple is from the angled flexible element (shown as C in Fig. 1). The bending moment, which balances this, is exhibited in the flexible element as a deformation. hence, blow-down. Experiments and numerical studies by Braun et al. [12] have consistently shown the presence of swirl at the seal exit.

3 Simple Flexible Element Analog

Widely spaced canted flexible strips as used in leaf seals demonstrate blow-down (see Fig. 2). A low speed wind tunnel with this geometrical arrangement was studied to highlight an aerody-

[1]Corresponding author.

Contributed by the International Gas Turbine Institute of ASME for publication in the JOURNAL OF TURBOMACHINERY. Manuscript received March 2, 2009; final manuscript received April 17, 2009; published online April 26, 2010. Review conducted by David Wisler. Paper presented at the ASME Turbo Expo 2008: Land, Sea and Air (GT2008), Berlin, Germany, June 9–13, 2008.

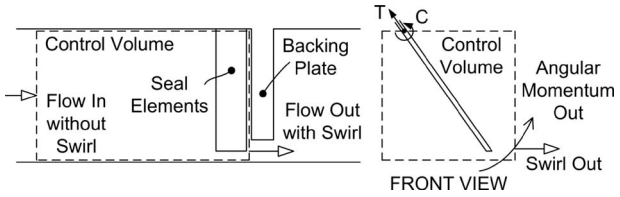

Fig. 1 Control volume for seal with angled elements

namic mechanism that generates blow-down. Comparisons between this idealized physical model and a numerical model were undertaken to isolate the mechanism.

3.1 Experimental Demonstration. A low speed wind tunnel with a 300×100 mm^2 working section was connected to a centrifugal in-line duct fan capable of creating a 400 Pa pressure difference. A number of 0.5 mm acrylic strips of 20 mm width and 90 mm free length were arranged at approximately 45 deg to the vertical, next to a backing plate in the working section (the normal spacing between the strips was 10 mm). When the air flow was activated, the strips exhibited blow-down, as shown in Fig. 2 (this compound image was created by extracting the lightest pixel value from both a stopped and flowing tunnel). The flow velocity of the wind tunnel was measured directly using a vane anemometer as 3.5 m s$^{-1} \pm 0.5$ m s^{-1} and indirectly as 3.5 m s^{-1} from a manometer reading of 7.5 Pa and by applying the Bernoulli equation. The Reynolds number based on the separation between the strips was 2700. Pressure measurements close to the backing ring suggested peak velocities in the region of 20–22 m s^{-1}. Small tufts were placed on the backing plate, the rotor surface, and the flexible strips. The flow-field captured is illustrated in Fig. 3. The key flow features seen are as follows:

1. downward fluid motion approaching leading edge
2. flow turning to align with strips
3. swirl induced by the inclination of the strips
4. flow separation vertically beneath strip tips
5. flow exiting strips with swirl
6. separation under backing plate and flow contraction
7. flow near floor aligned with axial direction

3.2 Numerical Model. In order to determine the origin of the blow-down force, it is only necessary to analyze the flow-field

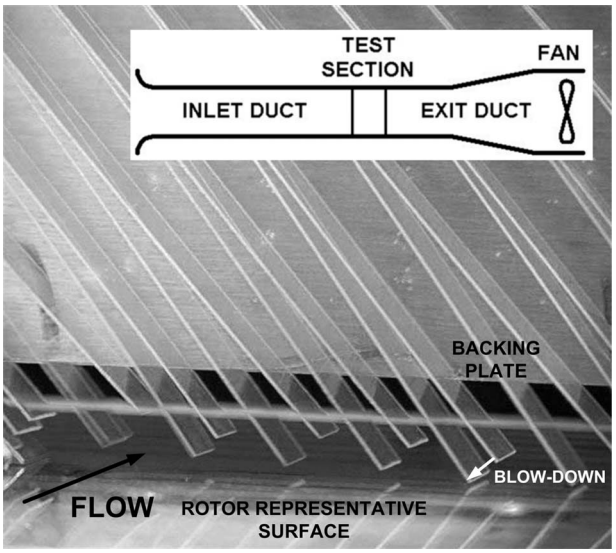

Fig. 2 Blow-down of thin widely spaced flexible leaves in a low speed wind tunnel

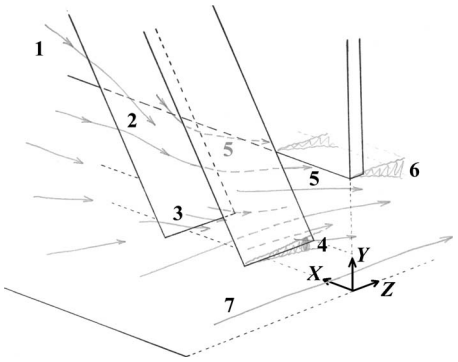

Fig. 3 Summary of flow-field main features from flow visualization

prior to blow-down (i.e., the known undeflected geometry). A simple computational domain was created for the flow between two zero thickness strips employing periodic boundary conditions. An unstructured tetrahedral mesh with increasing resolution toward the backing plate clearance was employed. The three-dimensional domain was solved using the FLUENT steady segregated implicit solver and the laminar viscous model with second order momentum discretization. Little change was detected when the number of cells was increased or when turbulence models were used. It should be emphasized that the key purpose of the numerical model was to confirm the presence of the aerodynamic mechanism as observed experimentally.

The static pressure contours over the upper and lower surfaces of the strips are shown in Fig. 4. If the pressure difference distribution is determined for the strip, then the magnitude of the blow-down pressure force can be established. Figure 5 shows that the blow-down locations peak at the leading and trailing edges at a height corresponding approximately to the backing plate height (the positive pressure difference corresponds to a blow-down direction). The pressure force term was found to be very much greater than the shear force term, confirming the insensitivity of the result to the turbulence model used. It is insightful to note the effect of a different lay angle on the blow-down pressure force. Figures 6 and 7 show the effect of a 30 deg and 60 deg lay angle on the form of the pressure difference distribution, respectively. Blow-down is reduced as the angle is reduced (as the strips become more vertical). The major change being that the leading edge blow-down force becomes less influential as the strips become more vertical. The numerical model confirms that the blow-down force is proportional to the inlet velocity squared, as expected from dimensional analysis.

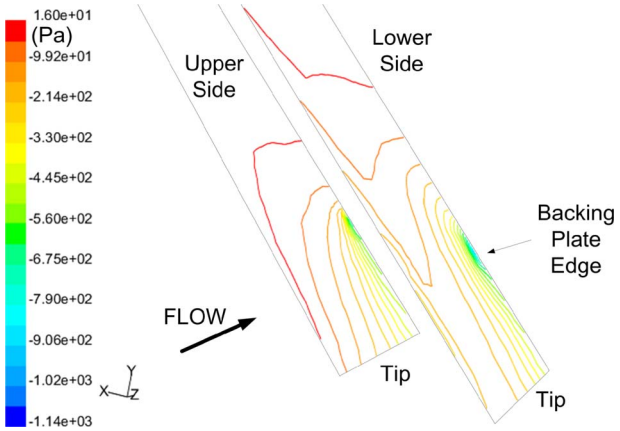

Fig. 4 Static pressure contours over the upper and lower surfaces of the canted strip

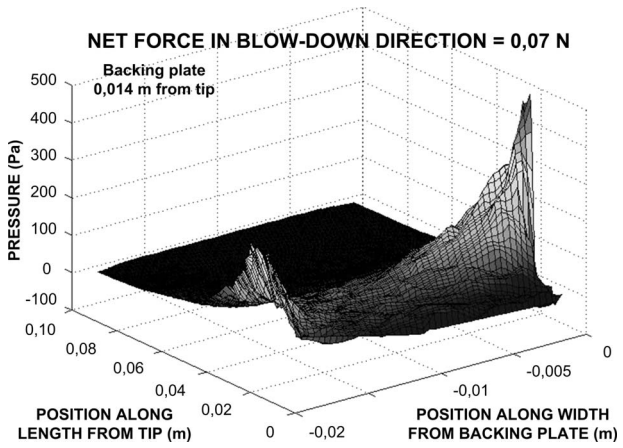

Fig. 5 Pressure difference distribution over the strip inclined at 45 deg

3.3 Blow-Down Mechanism. Blow-down on the inclined strips arises as a result of the flow changing direction on the approach to and exit from the strips. For steady flow, the momentum equation relates the net force acting on the fluid to the integral over the control surface of the net flux across the control volume boundaries. The shear force term was found to be very small compared with the pressure force term. Hence the net force can be considered to be the pressure force. Gravity will be neglected in this analysis.

Consider first the approach to the strips (the leading edge of the plates). Before the strips, the flow is aligned with the shaft surface in the axial direction and starts to turn vertically downwards toward the gap under the backing plate (as would be the case if there were no strips). Just after the leading edge of the inclined strips, the flow is forced to travel between the strips. This change in direction indicates that a pressure force is acting on the strips here. Consider a stream filament (between points 1 and 2 in Fig. 3), which is illustrated in detail in Fig. 8, showing a typical change in direction of a fluid element at the leading edge of the plates (element shown is on the upper surface). The flow along the small stream-tube can be considered like flow round a pipe bend. Hence the momentum equation can be applied in a similar way to that used in the analysis of a pipe bend. Note that α, the inlet approach angle, is measured in the plane of the inlet swirl defined by angle β. γ, the leaf entry angle, is measured in the plane of the leaves. When applied in the X (horizontal), Y (vertical), and Z (axial) directions for the inlet side of the strip, the momentum equation yields

$$F_X = (p_1 + \rho_1 u_1^2)\cos\ \alpha \sin\ \beta \delta A_1 - (p_2 + \rho_2 u_2^2)\cos\ \gamma \sin\ \theta \delta A_2 \tag{1}$$

$$F_Y = (p_1 + \rho_1 u_1^2)\sin\ \alpha \delta A_1 - (p_2 + \rho_2 u_2^2)\cos\ \gamma \cos\ \theta \delta A_2 \tag{2}$$

$$F_Z = -(p_1 + \rho_1 u_1^2)\cos\ \alpha \cos\ \beta \delta A_1 + (p_2 + \rho_2 u_2^2)\sin\ \gamma \delta A_2 \tag{3}$$

where F is the force exerted on the fluid by the strips and δA is the cross-sectional area of the stream-tube (p, ρ, and u refer to the fluid pressure, density, and velocity, respectively). The blow-down force is that exerted by the fluid on the strips and is evaluated locally on the strip using $F_Y \sin\ \theta - F_X \cos\ \theta$. The leading edge blow-down force follows as:

$$f_f = (p_1 + \rho_1 u_1^2)\,\delta A_1[\sin\ \alpha \sin\ \theta - \cos\ \alpha \cos\ \theta \sin\ \beta] \tag{4}$$

The equations suggest that the blow-down force will increase for high α and large θ. The second term is governed by the swirl, β, which could either act to reduce blow-down or increase it depending on the swirl direction relative to the lay angle. γ is not significant. Qualitatively, α will increase from zero at the floor of the tunnel to a maximum angle at around the midtunnel height. The velocity u_1 will increase toward the tunnel floor until the boundary layer is reached. Therefore the largest blow-down will occur on the leading edge when $u_1^2 \sin\ \alpha$ is a maximum (β, the swirl, is taken here to be zero, as was the case in the tunnel). This can be seen to correspond to a region just above the tip of the strips for many of the cases. When there are no strips present, the streamlines can be found from consideration of the potential function. Figure 9 presents the potential flow streamlines for a case of a backing plate only. The dashed outline shows where the strips would be positioned. This confirms the presence of a flow direction change suitable for generating a blow-down load, as postulated in Fig. 8. The density and angle of the streamlines in Fig. 9 also imply that the maximum blow-down at the leading edge occurs at the same position, as indicated by the numerical model.

Now consider the exit from the strips. The flow here sweeps off the inclined plates and under the backing plate with significant swirl. Consider a stream filament (regions 3 and 5 in Fig. 3) showing a change in direction of a fluid element at the trailing edge of the plates. Note that ϵ, the leaf exit angle, is measured in the plane of the leaves. The outlet escape angle, ζ, is measured in the plane of the outlet swirl, η. When applied in the X (horizontal), Y (vertical), and Z (axial) directions for the exit side of the strip, the momentum equation gives

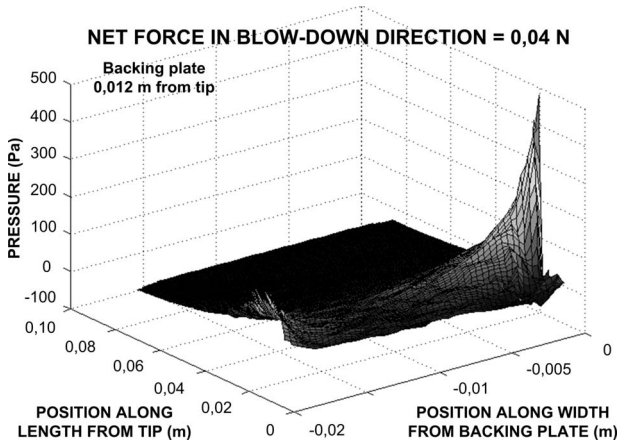

Fig. 6 Pressure difference distribution over the strip inclined at 30 deg

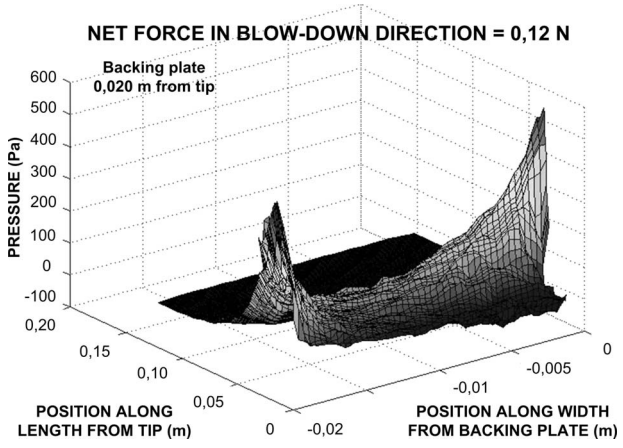

Fig. 7 Pressure difference distribution over the strip inclined at 60 deg

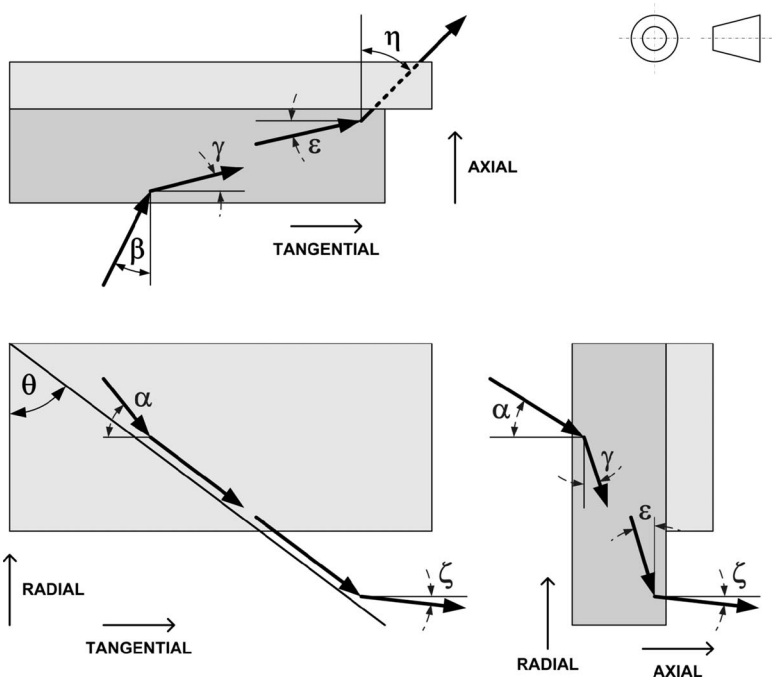

Fig. 8 Flow direction changes at the strip edges

$$F_X = (p_3 + \rho_3 u_3^2)\cos\ \epsilon\ \sin\ \theta \delta A_3 - (p_5 + \rho_5 u_5^2)\cos\ \zeta\ \sin\ \eta \delta A_5 \tag{5}$$

$$F_Y = (p_3 + \rho_3 u_3^2)\cos\ \epsilon\ \cos\ \theta \delta A_3 - (p_5 + \rho_5 u_5^2)\sin\ \zeta \delta A_5 \tag{6}$$

$$F_Z = -(p_3 + \rho_3 u_3^2)\sin\ \epsilon \delta A_3 + (p_5 + \rho_5 u_5^2)\cos\ \zeta\ \cos\ \eta \delta A_5 \tag{7}$$

The trailing edge blow-down is thus

$$f_b = (p_5 + \rho_5 u_5^2)\,\delta A_5[\cos\ \zeta\ \sin\ \eta\ \cos\ \theta - \sin\ \zeta\ \sin\ \theta] \tag{8}$$

The angle ζ is small and can be assumed to be zero for some, but not all, of the stream-tubes. Thus

$$f_b \approx (p_5 + \rho_5 u_5^2)\,\delta A_5[\sin\ \eta\ \cos\ \theta] \tag{9}$$

The analysis indicates that the blow-down force on the trailing edge is influenced by the exit swirl from the plates (this swirl is represented by angle η). The larger the swirl, the greater the blow-down force. The blow-down force on the trailing edge also depends on the bristle angle, θ. The presence of a small angle, ζ, due to the separation under the backing plate, reduces the blow-down force slightly. The angle ϵ does not appear in the expression for the blow-down force. The largest blow-down will occur where there is the greatest swirl from plates. This will occur at the free edge of the backing plate when much of the flow has been traveling along the plates. Further toward the tunnel floor, the flow is more aligned with the shaft axis than the plates so the blow-down force reduces. This is confirmed by the numerical model results (see Fig. 5).

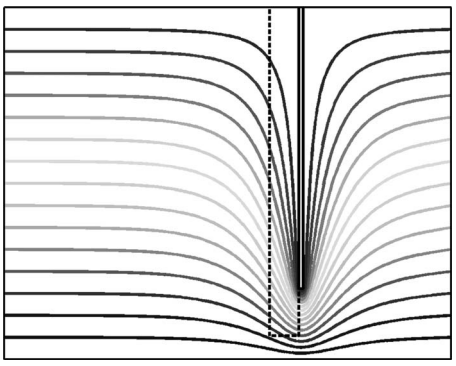

Fig. 9 Potential flow streamlines for case with no strips

These simple applications of the momentum equation can explain many of the computational predictions. The peak in pressure difference (between the upper and lower surfaces) on the trailing edge corresponds to a position just above the free edge of the backing plate. The leading edge pressure peak is less pronounced and is spread along the leading edge at around the level of the backing plate clearance. The theory would suggest that the relative magnitude of the leading and trailing edge pressure peaks would change as the angle θ is varied. For the 30 deg case, the trailing edge peak appears to be the only significant blow-down source, whereas for the 60 deg case the leading edge peak is almost the same size as the trailing edge peak (see Figs. 6 and 7). The swirl levels suggested by the numerical model, and confirmed by the tufting in the wind tunnel, point to the importance of swirl on the trailing edge blow-down.

4 Large Bristle Model

In order to simulate more closely the flow-field around the bristles in a brush seal prior to blow-down, a bristle pack consisting of eight rows of hexagonally close-packed nylon tubes was modeled. Pressures around the bristle surfaces were found by using rotatable tubes in the wind tunnel, as described below. The result of this experiment was compared with a numerical model created using computational fluid dynamics. The experiment was incompressible and hence did not exactly simulate the engine application. However, the inlet Reynolds number based on the bristle diameter was similar to that found in an engine.

4.1 Experimental Model. The test section (see Figs. 10 and 11) was placed in the same low-speed wind tunnel, as described earlier. Pressure measurements were taken on the surface of the bristles so that the flow-field could be quantitatively examined. Eight rows of hexagonally close-packed bristles canted at 45 deg were chosen to allow good replication of the flow features that are found in real brush seals (see Fig. 12). The bristles were made

Fig. 10 Large bristle pack in wind tunnel viewed from underneath

from 4 mm diameter nylon tubes and were sealed at the tips. A small side hole placed in a few of the tubes was used so that rotation of these tubes enabled pressure measurements to be made all around the bristle circumference (these bristles had a brass 45 deg foot to ensure that the rotation of the tapping did not change the tip geometry). Interchanging the instrumented bristles, each with the side hole at a different height, enabled a full picture of the pressure distribution in the bristle pack to be determined.

The inlet velocity was 1.40–1.45 m s^{-1}. Eight rotating bristles were used with tapping locations at 2.5 mm, 5 mm, 7.5 mm, 10 mm, 15 mm, 20 mm, 25 mm, and 45 mm from the tip. Measurements of pressure were made at eight angles around the circumference (0 deg, ±45 deg, ±90 deg, ±135 deg, and 180 deg). The uncertainty in the angle was well below ±5 deg and the vertical height of the tips of the instrumented bristles was within ±0.5 mm of the fixed bristle pack. Pressure measurements were taken using a water manometer to an accuracy within 3 Pa (1 Pa random error and 2.7 Pa systematic error using the 95% confidence level) after reaching a constant value for at least half a minute. The pressure distribution over the bristle surface for the first, second, and eighth row bristles is shown in Figs. 13–15, respectively (the first bristle row refers to the upstream or leading bristle row). The pressure is plotted versus distance from the tip, and the angle around the bristle is measured clockwise, as viewed from above, such that $+\pi/2$ faces upstream and 0 is the upper surface high-point. The measured pressure distribution around the cross section at 2.5 mm from the bristle tip is compared for bristles in rows 1, 2, and 8 in Fig. 16 (the 2.5 mm refers to the closest distance between the bristle perpendicular cross section and the bristle tip). The measured pressure distributions were integrated over the bristle sur-

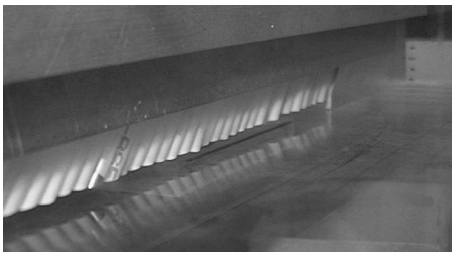

Fig. 11 Large bristle pack in wind tunnel viewed from exit plenum chamber

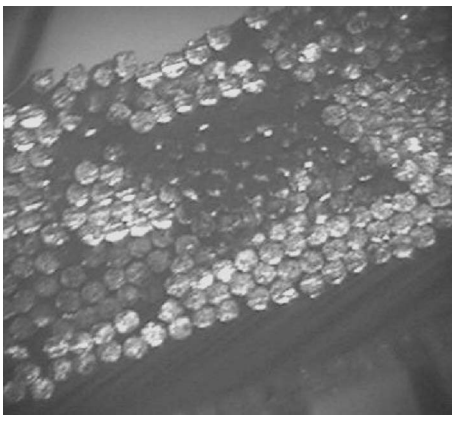

Fig. 12 Enlarged image of real brush seal packing

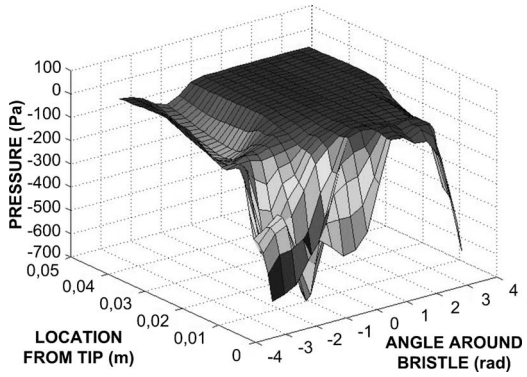

Fig. 13 Pressure distribution measured over bristle surface (row 1)

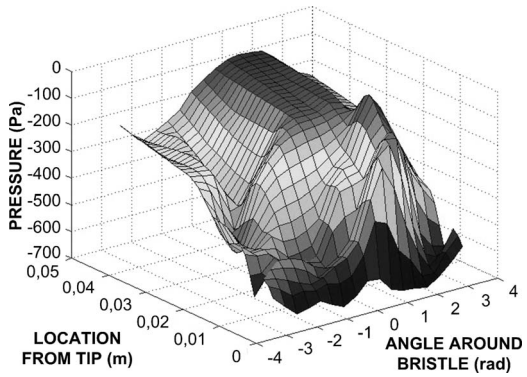

Fig. 14 Pressure distribution measured over bristle surface (row 2)

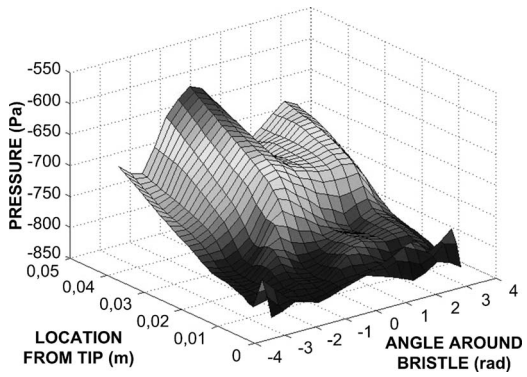

Fig. 15 Pressure distribution measured over bristle surface (row 8)

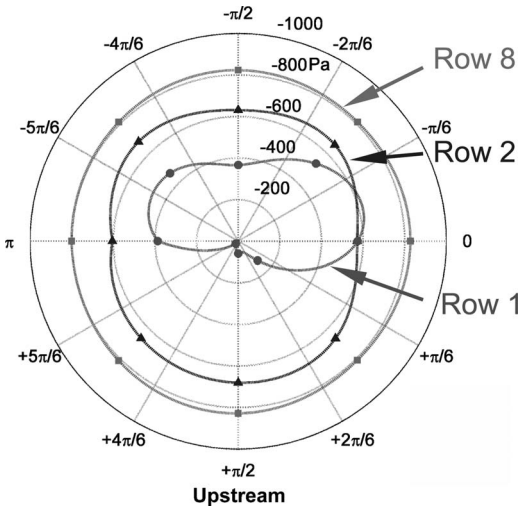

Fig. 16 Variation in pressure around bristle cross section at 2.5 mm minimum distance from tip

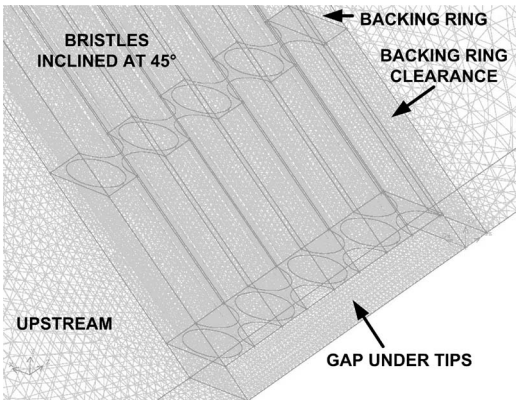

Fig. 17 Detail of the mesh around the bristle tips

face to determine the net pressure force on the bristles. A blow-down force and an axial force (force in main flow direction) were found to be present on each bristle.

4.2 Numerical Model. A similar numerical approach was adopted for the large scale bristle pack to that used in the simple flexible element analog. A number of grids using unstructured tetrahedral elements with increasing resolution toward the bristle tips and in the bristle-to-rotor clearance zone were used. Periodic boundaries were implemented. Figure 17 illustrates an example grid. A fixed bristle-to-bristle separation of 0.2 mm was initially assumed for the numerical model (the interbristle separation was both difficult to measure and changed during wind tunnel operation, so a number of other fixed bristle-to-bristle separations were also modeled). As before, the FLUENT steady segregated implicit solver was run on the three-dimensional domain. The flow was treated as laminar and incompressible and second order momentum discretization was implemented. The viscous force acting on the bristle surfaces was found to be much less than 10% of the total force so that the static pressure alone was deemed to give a good first approximation to the bristle loading.

Figure 18 shows the flow squeezing between the bristles and under the backing plate on the midchannel plane (this plane cuts through the bristles in the odd rows and the gaps in the even rows, and the backing plate is cut through on the right of the figure). Velocity vectors on an axial plane inside the bristle pack are presented in Fig. 19. A vortex can be seen forming under the central bristle. The downward flow here originates from the void just upstream of this point (see inset in Fig. 19). The flow in the rest of the clearance region under the bristles is fast and axially directed with slight swirl toward the right. Analysis of the static pressure distributions around each bristle row confirmed that a net axial force and a net blow-down force existed on each bristle. The net blow-down force is presented in Fig. 20.

4.3 Comparison Between Physical and Numerical Models. A quantitative assessment of the effect of the separation on the pressure field was carried out by running the numerical model with interbristle spacings of 0.2 mm, 0.3 mm, and 0.4 mm with an inlet velocity of 1.9 m s^{-1} (required to match the volume flow rate in the experiment). The relationship is not linear (see Fig. 20). The blow-down loads generally increase with the bristle row number and increase with reducing interbristle separation, with a marked increase from 0.3 mm to 0.2 mm. The pressures around the bristle surfaces for these three cases were compared with the data obtained from the wind tunnel tests. Figures 21 and 22 illustrate that reasonably good agreement was found. Note that the area of the tapping was quite large compared with the size of the small pressure variations, implying some integration of results. Discrepancies between the physical and numerical model pressure distributions were largely due to the movement of the bristles (and

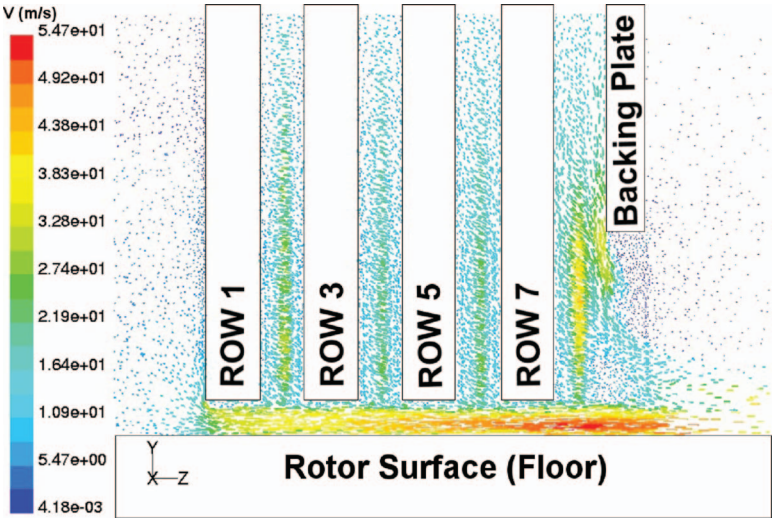

Fig. 18 Velocity vectors on the midchannel plane viewed from the side

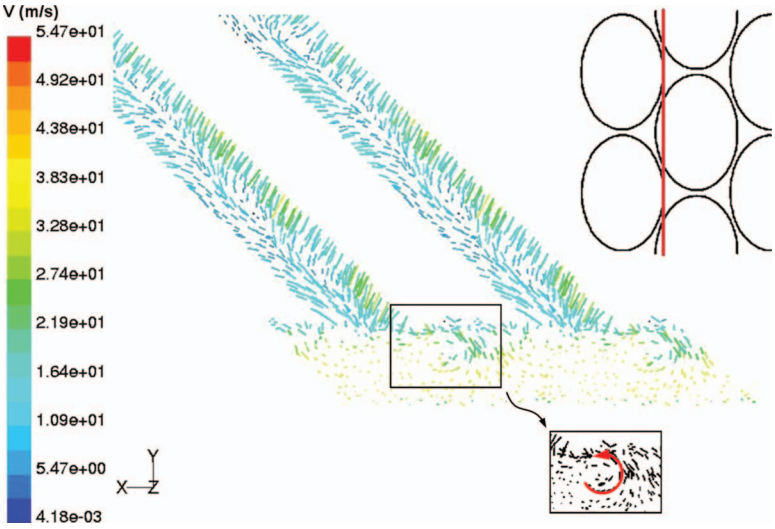

Fig. 19 Velocity vectors on the indicated axial plane viewed from the inlet

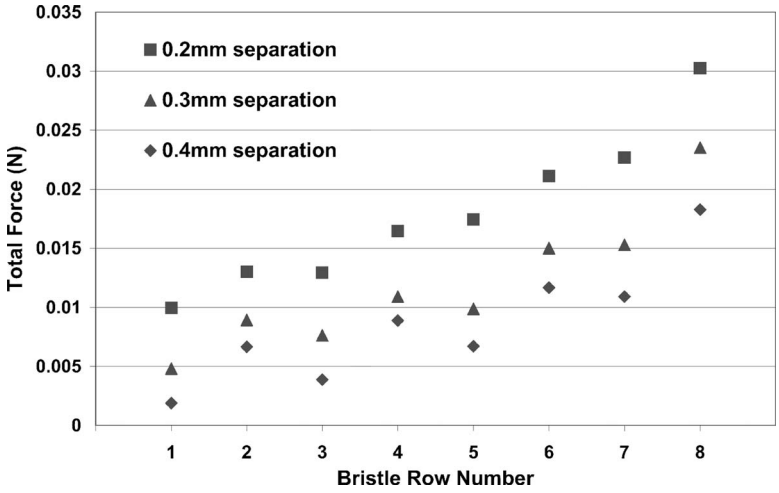

Fig. 20 Force acting on each bristle in the blow-down direction (1–10)

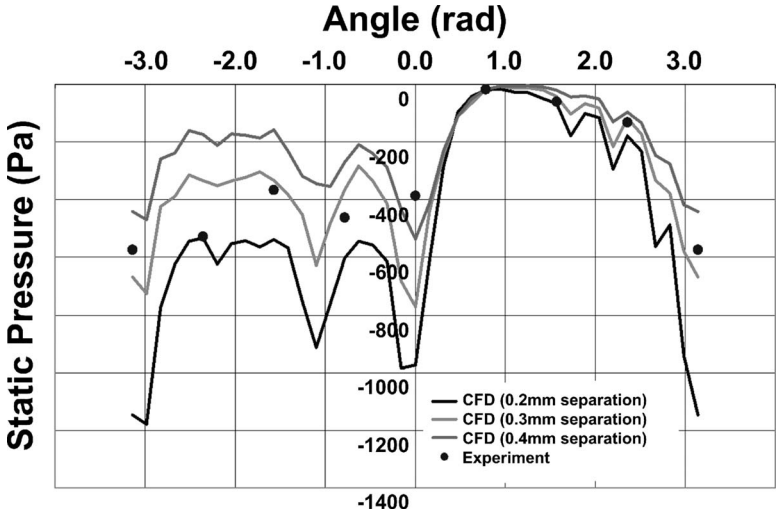

Fig. 21 Comparison between CFD and experiment (first row bristle at 2.5 mm from tip)

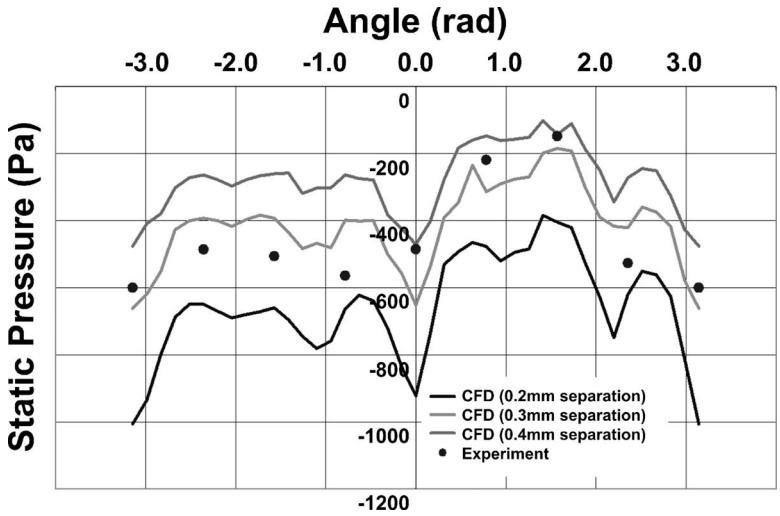

Fig. 22 Comparison between CFD and experiment (second row bristle at 7.5 mm from tip)

consequent modification of the bristle spacing throughout the pack), as well as the difficulty in controlling the interbristle spacing during manufacture. The results emphasize that the interbristle separation is a key parameter governing the flow. Studies dedicated to the numerical simulation of brush seal flow have noted the difficulty in choosing the appropriate porosity values or spacings [10,13].

4.4 Bristle Blow-Down. When the thickness of the flexible elements can no longer be assumed to be zero, there is potential for an additional blow-down loading term. The pressure field through a typical bristle pack has a higher pressure closer to the bristle root and lower pressure toward the bristle tips where the backing plate clearance (flow outlet) is. This vertical pressure gradient creates a pressure mismatch on either side of the flexible element, as illustrated in Fig. 23 (assuming the pressures are approximately equal normal to the bristle surface where the streamlines are parallel and that the flow field is identical at the periodic boundaries). Such a pressure mismatch between the two sides of the element will produce a bending moment and so a blow-down moment will result for the case when the pressure is generally decreasing from root to tip.

Examination of the velocity vectors obtained from the computational simulation indicates some of the mechanisms that contribute toward bristle blow-down. The front bristle row experiences tip blow-down as the flow close to the tip speeds under the bristle on the lower surface side and creates a lower pressure there. The upper surface has no such effect and so has a higher pressure, enabling blow-down. Flow direction changes occurring in the middle of the bristle pack account for a proportion of the blow-down load. These direction changes can be analyzed by considering the flow round the upper surface and the flow round the lower surface of the bristles (see Fig. 24). Given that, for this large scale model, the pressure forces dominate the shear forces then the momentum equation applied only for the velocity changes will capture blow-down. Figures 25 and 26 depict the velocity changes around the upper and lower surfaces of the bristle, respectively. Applying the momentum equation in the X and Y directions and noting that the blow-down force is $F_Y \sin\theta - F_X \cos\theta$ gives the upper and lower surface blow-down loads as Eqs. (10) and (11), respectively.

$$f_u = -(p_1 + \rho_1 u_1^2)\delta A_1 \sin\lambda \cos(\theta + \kappa) - (p_2 + \rho_2 u_2^2)\delta A_2 \sin\nu \cos(\theta + \mu) \tag{10}$$

$$f_l = (p_3 + \rho_3 u_3^2)\delta A_3 \sin\chi \sin(\theta + \phi) + (p_4 + \rho_4 u_4^2)\delta A_4 \sin\omega \cos(\theta + \psi) \tag{11}$$

Note that the upper surface blow-down load effectively produces a lifting force. The net blow-down force just from consideration of these two stream filaments would be zero if condition 1 equals 4 and 2 equals 3. This would only be the case for flow through an infinite array of angled bristles where there is no vertical (radial) pressure gradient. In fact, the numerical simulation suggests that the velocity of 3 is much higher than that of 1. Consideration of these stream filaments emphasizes the finding of the numerical

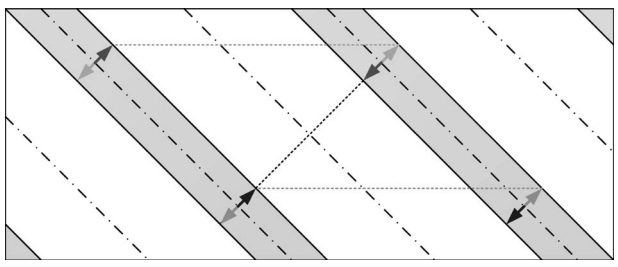

Fig. 23 Pressure field mismatch between the sides of a flexible element with thickness

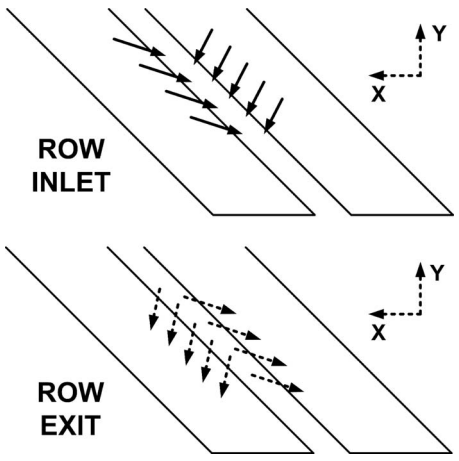

Fig. 24 Velocity vectors at the inlet and exit from internal rows of bristles

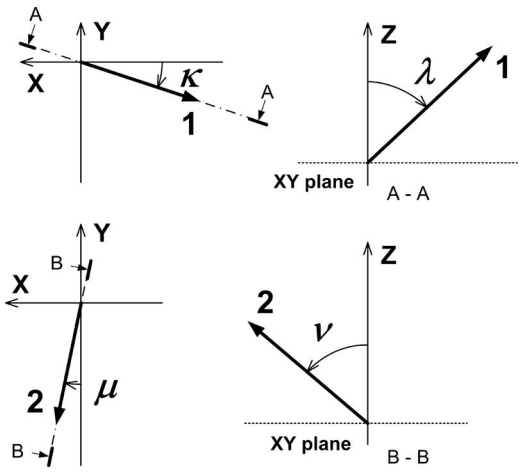

Fig. 25 Flow directions at the inlet to (top) and exit from (bottom) a stream filament around the upper surface of the bristle

model: that most of the blow-down force occurs toward the bristle tip. At the tip, flow leaves the pack aligned with the bristle axes and contributes to the swirl in the clearance region under the bristles. Here, the lower surface stream tube contributes more to f than the upper surface stream tube, and a net blow-down force results. The exiting flow reduces the amount of flow at the inlet to the next row. The final row has a large blow-down force due to the flow escaping with significant swirl under the backing plate clearance. The angle of escape (vertical velocity) of this flow is also important, especially just under the backing plate.

Consider the effect of a change in bristle-to-rotor clearance on blow-down for clearance seals. A reduction in bristle clearance requires that a greater length of the flexible filaments protrude into the backing ring clearance zone (the backing ring clearance being fixed). This produces additional swirl leading to a higher exit swirl velocity. The control volume analysis presented suggests that a higher exit swirl velocity will induce greater blow-down. The numerical model for the simple flexible element analog confirms this with an increase in blow-down load of 7% for a reduction in clearance from 5 mm to 1 mm.

It can be seen that it is not necessary for the bristle pack to deform to generate a blow-down load. The origin of the load has been explained for a fixed array of bristles or for a fixed array of inclined flexible elements (strips or leaves). Some previous studies [9,14,15] have linked blow-down to axial forces through what is generally termed the *inclined prop effect*. This would require the bristle to deflect axially. The normal reaction of bristle-to-backing plate contact can be modeled as a point contact between the bristle and the backing plate edge. If the bristle deflects under the backing plate, then the normal contact force will rotate with the bristle and then it is possible to transfer part of the axial loading into a radial force component, which can act to move the bristle radially inwards. However, the current research suggests that the aerodynamic forces are of sufficient level to generate a large proportion of the blow-down load for brush seals and virtually all the load for axially stiff seals, such as leaf seals, where contact with the backing plate does not normally occur.

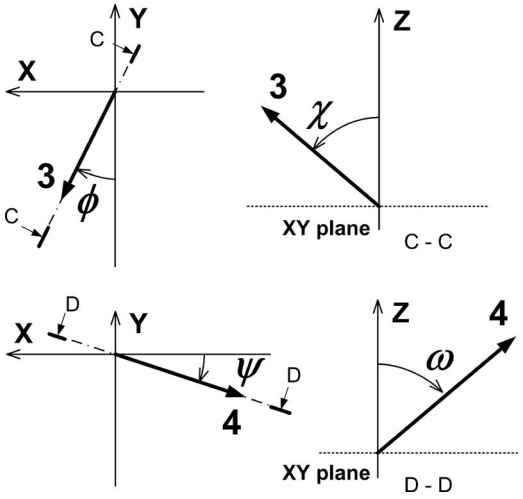

Fig. 26 Flow directions at the inlet to (top) and exit from (bottom) a stream filament around the upper surface of the bristle

5 Summary and Conclusions

Aerodynamic reasons for blow-down in compliant filament seals have been investigated by examining the flow-field in a simple flexible element analog and a more realistic model of a bristle pack. Wind tunnel tests and numerical models, whose results were consistently in good agreement, were used to identify some important aerodynamic mechanisms that can generate blow-down. Numerical modeling showed that pressure forces dominate over shear forces: thus measured pressures were used to infer forces on the seal elements. In the case of a bristle pack, inter-bristle spacing was seen to have a great effect on the flow-field.

For all adaptable seals comprising compliant flexible elements, the blow-down effect is driven by differential pressure rather than pressure ratio. In the case of zero thickness inclined strips, it is brought about by momentum changes alone. For flexible elements that have thickness, a blow-down moment is generated in the presence of a vertical (radial) pressure gradient (pressure generally decreasing from root to tip). Blow-down due to flow momentum changes in a brush seal can be described as follows. Flow, initially aligned with the shaft axis, starts to turn toward the shaft surface in anticipation of the impending area reduction under the backing plate. Flow approaching the bristles is turned to align with the bristles and enters the bristle pack. The fluid close to the tips exits into the channel under the tips and contributes toward the swirl in this region. In doing so, a pressure distribution is created around the tips, which produces a blow-down force. The swirl from the final row of bristles under the backing plate results in a greater blow-down force for this row.

Acknowledgment

Assistance and advice was gratefully received from Dr. Jonathan Morgan and Professor John Chew. The experimental apparatus was manufactured by staff at the Department of Engineering Science, University of Oxford. Their support is greatly appreciated.

Nomenclature

A = cross-sectional area, m^2
a = pressure fraction
C = couple or bending moment, N m
F = force, N
f = blow-down force, N
p = pressure, Pa
p_{up} = upstream pressure, Pa
p_{down} = downstream pressure, Pa
T = tension, N
u = velocity, m s^{-1}
X = horizontal coordinate direction
Y = vertical coordinate direction
Z = axial coordinate direction
α = inlet approach angle, rad
β = inlet swirl angle, rad
γ = strip entry angle, rad

ϵ = strip exit angle, rad
ζ = outlet escape angle, rad
η = outlet swirl angle, rad
θ = lay angle radial, rad
ρ = density, kg m^{-3}

References

[1] Ferguson, J., and Waters, G., 1975, "Seals and Method of Manufacture Thereof," United States Patent No. US0003917150.

[2] Chupp, R., Prior, R., and Lowenthal, R., 1996, "Update on Brush Seal Development for Large Industrial Gas Turbines," *AIAA/SAE/ASME/ASEE Joint Propulsion Conference and Exhibit*, Lake Buena Vista, FL, AIAA, Reston, VA, Vol. 32, Paper No. 96-3306.

[3] Wolfe, C. E., Chiu, R. P., Cromer, R. H., Crum, G. A., Marks, P. T., Stuck, A. E., Turnquist, N. A., Reluzco, G., and Dinc, O. S., 1997, "Brush Seals in Industrial Gas Turbines," *AIAA/SAE/ASME/ASEE Joint Propulsion Conference and Exhibit*, Seattle, WA, AIAA, Reston, VA, Vol. 33, Paper No. 97-2730.

[4] Dinc, O., Demiroglu, M., Turnquist, N., Mortzheim, J., Goetze, G., Maupin, J., Hopkins, J., Wolfe, C., and Florin, M., 2001, "Fundamental Design Issues of Brush Seals for Industrial Applications," ASME Paper No. 2001-GT-0400.

[5] Ferguson, J. G., 1988, "Brushes as High Performance Gas Turbine Seals," ASME Paper No. 88-GT-182.

[6] Nakane, H., Maekawa, A., Akita, E., Akagi, K., Nakano, T., Nishimoto, S., Hashimoto, S., Shinohara, T., and Uehara, H., 2002, "The Development of High Performance Leaf Seals," ASME Paper No. 2002-GT-30243.

[7] Bayley, F. J., and Long, C. A., 1993, "A Combined Experimental and Theoretical Study of Flow and Pressure Distributions in a Brush Seal," ASME J. Eng. Gas Turbines Power, **115**(2), pp. 404–410.

[8] Wood, P. E., and Jones, T. V., 1999, "A Test Facility for the Measurement of Torques at the Shaft to Seal Interface in Brush Seals," ASME J. Eng. Gas Turbines Power, **121**, pp. 160–166.

[9] Lelli, D., Chew, J. W., and Cooper, P., 2005, "Combined 3D Fluid Dynamics and Mechanical Modelling of Brush Seals," ASME Paper No. GT2005-68973.

[10] Chen, L. H., Wood, P. E., Jones, T. V., and Chew, J. W., 2000, "Detailed Experimental Studies of Flow in Large Scale Brush Seal Model and a Comparison With CFD Predictions," ASME J. Eng. Gas Turbines Power, **122**, pp. 672–679.

[11] Turner, M. T., Chew, J. W., and Long, C. A., 1997, "Experimental Investigation and Mathematical Modelling of Clearance Brush Seals," ASME Paper No. 97-GT-282.

[12] Braun, M. J., Canacci, V. A., and Hendricks, R. C., 1992, "Flow Visualization and Motion Analysis for a Series of Four Sequential Brush Seals," J. Propul. Power, **8**(3), pp. 697–702.

[13] Demiroglu, M., Aksit, M. F., and Tichy, J. A., 1998, "A Numerical Study of Brush Seal Leakage Flow," *Joint Propulsion Conference and Exhibit, AIAA/SAE/ASME/ASEE*, Cleveland, OH, AIAA, Reston, VA, Vol. 34, Paper No. 98-3173.

[14] Chen, L. H., Wood, P. E., Jones, T. V., and Chew, J. W., 1998, "An Iterative CFD and Mechanical Brush Seal Model and Comparison With Experimental Results," ASME Paper No. 98-GT-372.

[15] Crudgington, P., and Bowsher, A., 2003, "Brush Seal Blow Down," *AIAA/SAE/ASME/ASEE Joint Propulsion Conference and Exhibit*, Huntsville, AL, AIAA, Reston, VA, Vol. 39, Paper No. 2003-4697.